Optimization of printing parameters using Taguchi method to improve the quality of parts produced by Metal Binder Jetting

Marco Zago[1][0000-0002-2798-5482] and Ilaria Cristofolini[1][0000-0003-2787-1271]

[1] Department of Industrial Engineering, University of Trento, Via Sommarive 9, 38123 - Trento, Italy
marco.zago-1@unitn.it

Abstract. This work aims at improving the quality, meaning both dimensional accuracy and green density, of binder jetting products by the optimization of printing parameters. Cubes with a squared through hole were printed using AISI 316L stainless steel powder, varying four printing parameters: dark body (binder saturation), shell thickness, printhead, and powder spreading speed. Taguchi methodology was employed to design nine orthogonal experiments, permutating the four factors at three levels. The green density was measured by mass to volume ratio, and the dimensions of the printed parts were derived by coordinate measuring machine (CMM) measurements. Green density and dimensional accuracy were the response variables to be optimized.
It was observed that green density varied in the interval (0.53÷0.57) of relative density; ANOVA (ANalysis Of VAriance) showed that the highest contribution to maximize green density (81%) is given by dark body. Concerning dimensional accuracy, the difference between measured and nominal dimensions, referred to nominal dimensions, varied between 0.53% and -1.01%. Dimensions parallel to binder injection direction (X) are mostly affected by shell thickness and dark body (35% and 55%, respectively). Printhead speed and powder application speed, instead, mostly affect dimensions parallel to powder spreading direction (Y) and dimensions aligned with building direction (Z) - printhead speed 56% for Y and 37% for Z, powder application speed 30% for Y and 24% for Z, respectively. A physical explanation is discussed, moreover linear regression models are proposed for optimizing parameters.

Keywords: Additive Manufacturing, Design of Experiment, Dimensional Accuracy.

1 Introduction

ASTM standards categorize seven types of additive manufacturing (AM) processes [1]. Among them, Binder Jetting (BJ) attracts significant attention for its high scalability, high production rate and the virtual processability of any ceramic and metallic materials [2][3]. BJ parts are produced layer-by-layer by selectively injecting a binder agent onto

a powder bed. After printing, thermal treatments are mandatory to burn-out the binder (de-binding) and consolidate particle structure (sintering), also closing porosity.

The widespread adoption of BJ is currently restricted by the challenging control of shape accuracy after sintering [4]. This reason can be ascribed to the detrimental effect of anisotropic shrinkage [5]**;** moreover, shape distortion can also occur due to gravity-induced load and the viscous material behavior on sintering [6]. In general, literature reports a lower tolerance grade with respect to metal injection molding [7].

Several authors have investigated the optimization of BJ process using design of experiment approach. Barthel studied five factors (layer thickness, roller diameter, supply-to-spread ratio, translation and rotational speed) at two levels to optimize green and sintered density [8]. Wang and Zhao analyzed the effects of sintering temperature, time and heating rate on accuracy of 316L products [9]. Chen et al also focused on maximizing sintered density of 316L [10]**,** whereas Shrestha and Manogharan analyzed the best printing parameters to increase transverse rupture strength [11]. Lores et al focused on the optimization of surface roughness of Invar36 Fe-Ni alloy by L9 orthogonal experiments [12]. Chen and Zhao investigated 420 stainless steel to minimize surface roughness and the inaccuracy of sintered product [13]. In other works alumina [14] and NCKU-1 powders [15] were studied.

The dimensional accuracy of final sintered product is detrimentally affected by the lack of precision at green state, as observed in [16][17]. However, the quality of the green products, referring to dimensional accuracy and green density, is not largely investigated in literature. For this reason, this work aims at optimizing the printing parameters to maximize product accuracy and green density. A Taguchi method L9 was used to assess the effect of four parameters at three levels. Six response variables were calculated: five for dimensional accuracy and one for green density. Optimal levels were identified analyzing signal-to-noise ratio and parameters' contribution by ANOVA. Finally, a linear regression model was estimated to optimize each response variable.

2 Materials and Methods

A cube with squared through-hole was designed, as shown in Fig. 1; the datum system in the printing box allows recognizing the directions related to the investigated parameters, where:

- X corresponds to binder injection direction;
- Y corresponds to powder spreading direction;
- Z corresponds to building direction.

STL file was imported into Materialise Magic software suite, and 36 parts each batch were replicated in the building volume in different positions.

The numeric marker printed on the samples surface shown in Fig. 1 allows distinguishing both the orientation with respect to the datum system XYZ, and the position in the printing box, after de-powdering.

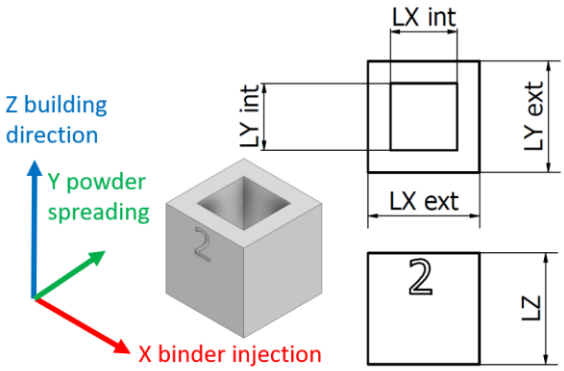

Fig. 1. Sample geometry and main features according to reference system.

The geometry was scaled using the parameters suggested by the company producing the printing machine, to take into account the expected anisotropic shrinkage during sintering; the resulting nominal dimensions in the green state are reported in **Table 1**.

Table 1. Nominal dimensions - scaled geometry. Dimension annotation according to **Fig. 1**.

LX-ext [mm]	LX-int [mm]	LY-ext [mm]	LY-int [mm]	LZ [mm]
11.99	7.13	12.07	7.24	12.37

Stainless steel 316L powder with D50 of 8.1 µm was used in this study. Samples were fabricated by a Digital Metals P1701 printing machine. Four printing parameters were investigated, namely:

- Speed (F1): it corresponds to the speed of the printhead along X direction.
- Dark body (F2): for each layer, the sample section is divided into a shell and a core area. A different amount of binder can be deposited in the shell and core area. Different binder amount in the core was selected as factor parameter. For sake of clarity, dark body index equals to 3 means that 69% of the pixels in the core is covered by binder [18].
- Powder applicator speed (F3): it is the speed of the rake during the powder spreading operation.
- Shell thickness (F4): as mentioned, sample section is divided in a shell and core area. The shell thickness controls the size of the shell. Dark index equals to 8 was kept for the shell area.

Other parameters were kept constant in this study. Layer thickness was set to 42 µm, with resolution of 1200 dpi and powder bed temperature equal to 80 °C.
The optimization of printing parameters was performed using Taguchi method. This DoE approach helps to determine the influence of factors while reducing the number of tests. For example, the combination of four factors varying at three levels can be studied

with an orthogonal array of 9 tests (L9), instead of 81 tests as required for a full factorial analysis [19]. The L9 matrix was designed and reported in Table 2.

Table 2. Factors and levels investigated.

Factors	Factor ID	Levels		
		1	2	3
Speed [mm/s]	F1	150	200	250
Dark body [-]	F2	0	3	6
Powder applicator speed [mm/s]	F3	25	30	38
Shell Thickness [pixel]	F4	1	3	5

Nine batches were printed using the combination of parameters reported in Table 3.

Table 3. Matrix L9 of experiments according to Taguchi method.

N°experiment	Levels			
	Speed	Dark Body	Powder Applicator Speed	Shell Thickness
1	1	1	1	1
2	1	2	2	2
3	1	3	3	3
4	2	1	2	3
5	2	2	3	1
6	2	3	1	2
7	3	1	3	2
8	3	2	1	3
9	3	3	2	1

After printing, the building box was cured, and subsequently de-powdered to extract the green samples. For each sample, the geometry was reconstructed by Coordinate Measuring Machine (CMM) to derive the actual dimensions. The surfaces defining the boundary of samples were measured by point-by-point strategy. Planes were then reconstructed by least squares method. Dimensions were derived from the distance between opposing planes. Inaccuracy was calculated by equation (1).

$$\boldsymbol{inaccuracy} = \frac{\boldsymbol{L_{Meas} - L_{Nom}}}{\boldsymbol{L_{Nom}}} \tag{1}$$

Where *L* corresponds to the dimensions shown in Fig. 1, while subscripts *Meas* and *Nom* correspond to the dimensions measured by the CMM and to the nominal dimensions reported in **Table 1**, respectively. By this criterion, dimensional error can be easily evaluated and used in the Taguchi method, moreover external and internal features can be compared along three directions by the normalization. The sample volume was also derived using the geometry reconstructed by measurement. The green density was calculated by equation (2).

$$\boldsymbol{Green\ Density} = \frac{\boldsymbol{weigth\ of\ green\ part}}{\boldsymbol{Volume\ of\ green\ part}} \quad (2)$$

The dimensions derived for the 36 replicates were then averaged for each batch. Density and inaccuracy were defined as the response variables to be used in Taguchi analysis performed by Minitab software analyzing signal-to-noise ratio (SNR) and ANOVA. A "smaller is better" quality loss function was related to SNR for evaluating inaccuracy (equation 3), whereas a "bigger is the better" quality loss function was used for evaluating green density (equation 4).

$$\boldsymbol{S/N_{inaccuracy}} = -\mathbf{10}\,\boldsymbol{log_{10}}\left(\frac{\mathbf{1}}{\boldsymbol{n}}\sum_{\boldsymbol{i=1}}^{\boldsymbol{n}}\boldsymbol{y_i^2}\right) \quad (3)$$

$$\boldsymbol{S/N_{density}} = -\mathbf{10}\,\boldsymbol{log_{10}}\left(\frac{\mathbf{1}}{\boldsymbol{n}}\sum_{\boldsymbol{i=1}}^{\boldsymbol{n}}\frac{\mathbf{1}}{\boldsymbol{y_i^2}}\right) \quad (4)$$

Finally, a linear regression model was used to predict optimum process parameters, as expressed by equation (5).

$$\boldsymbol{Response\ variable} = \boldsymbol{\alpha} + \boldsymbol{F1\beta} + \boldsymbol{F2\gamma} + \boldsymbol{F3\delta} + \boldsymbol{F4\zeta} \quad (5)$$

3 Results and Discussion

Table 4 reports the green density and dimensional inaccuracy, specifically the average and standard deviation calculated for the 36 samples of each batch/experiment. Further work will discuss the accuracy function of part location, and the statistical analysis such as the range, median, and outlier assuming normal distribution.

Table 4. Green density and dimensional inaccuracy for each batch. Standard deviation is reported between brackets.

Batch	Density [g/cm^3]	LXext [%]	LYext [%]	LXint [%]	LYint [%]	LZ [%]
1	4.31 (0.07)	0.53 (0.21)	0.19 (0.15)	-0.90 (0.16)	-0.52 (0.32)	0.31 (0.28)
2	4.42 (0.07)	0.47 (0.21)	0.08 (0.11)	-0.99 (0.17)	-0.45 (0.17)	0.47 (0.24)
3	4.45 (0.07)	0.34 (0.19)	-0.12 (0.09)	-0.85 (0.15)	-0.45 (0.13)	0.31 (0.26)
4	4.19 (0.07)	0.39 (0.19)	0.01 (0.08)	-0.75 (0.11)	-0.48 (0.17)	0.33 (0.32)
5	4.39 (0.04)	0.45 (0.19)	-0.04 (0.08)	-0.90 (0.14)	-0.55 (0.19)	0.31 (0.16)
6	4.54 (0.07)	0.49 (0.19)	0.05 (0.11)	-1.02 (0.14)	-0.54 (0.30)	0.29 (0.21)

7	4.10 (0.06)	0.41 (0.18)	0.02 (0.09)	-0.81 (0.10)	-0.32 (0.26)	0.01 (0.25)
8	4.50 (0.05)	0.32 (0.19)	0.10 (0.11)	-0.88 (0.13)	-0.81 (0.17)	0.26 (0.22)
9	4.58 (0.04)	0.39 (0.19)	-0.04 (0.14)	-1.01 (0.14)	-0.73 (0.19)	0.24 (0.20)

Green density varies between 4.10 and 4.54 g/cm^3, corresponding to an interval between 0.53 and 0.57 of relative density. The data is consistent with literature [20][21] for 316L BJ stainless steel.

Except for external features in Y direction, the accuracy along building direction (Z) is slightly better with respect to the building plane. This result was unexpected because the resolution along building direction (layer thickness of 42 μm) is significantly lower than on the building plane (1200 DPI approximately correspond to 21 μm). In XY plane, dimensions are more accurate along Y than X direction, both external and internal. Parab et al observed the ballistic impact of binder droplets and the consequence ejection of particles from the powder bed [22]. Thus, particles rearrangement might have caused different precision in the building plane. Further analysis of Table 4 shows that inaccuracy is generally positive along Z and X, Y (external features), whereas it is constantly negative along X and Y internal features. This behavior can be related to an excess of binder saturation used on the shell surface. Basically, it is supposed that binder could have migrated out of nominal shape, bonding extra powders and determining bigger dimensions. The data seems constant in all the batches, not directly related to saturation index used for the core area. By contrast, inaccuracy along powder spreading direction (Y) varied around zero. Future study should clarify this trend.

Fig. 2 reports the signal-to-noise ratio for the five response variables: the green density and the inaccuracy of all the dimensions (LX-ext, LX-int, LY-ext, LY-int, and LZ). Optimal levels are highlighted by a red square marker.

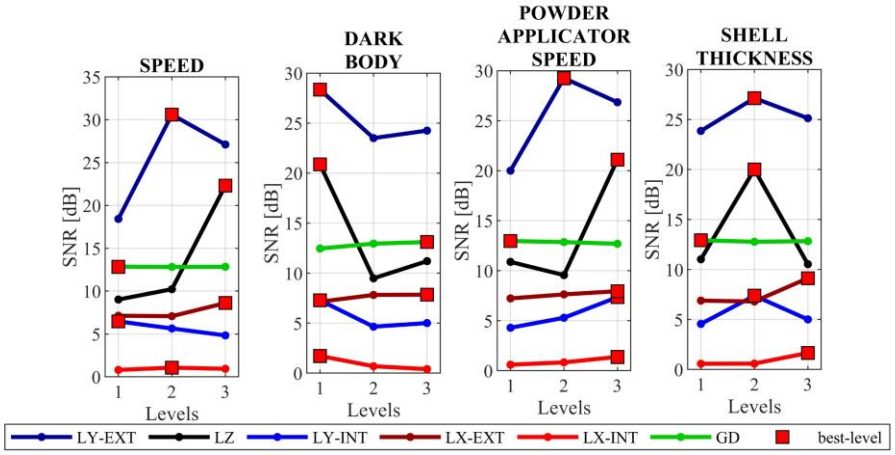

Fig. 2. Signal-to-noise (ratio SNR) of green density and inaccuracy response.

Generally, the optimal combination of parameters is a function of the response variables. The optimal levels for minimizing inaccuracy were found to vary for external and internal features, as well as for features aligned in the same direction. As an example, strictly speaking the lowest level for dark body would be needed for optimizing the accuracy of LY-ext, LY-int, LZ and LX-int, while the highest level for dark body would be needed for optimizing green density and LX-ext. Further studies will investigate multivariable optimization to identify the best parameter combination.
The relative importance of the different factors has also to be considered, as further highlighted by ANOVA.

Fig. 3 shows the contribution of each factor to the response variables as derived by ANOVA.

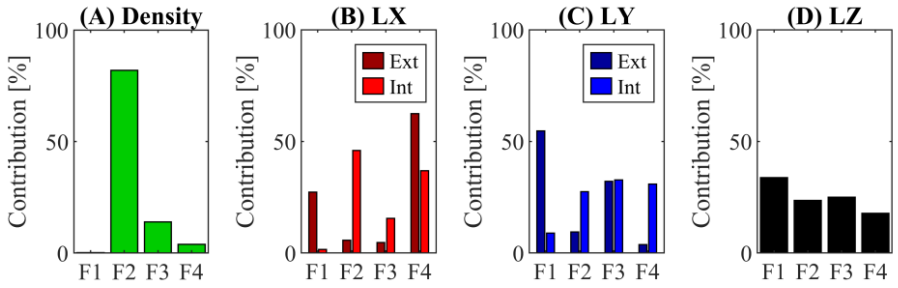

Fig. 3. Contribution of each factor to response variable optimization: (A) green density, dimensional inaccuracy of (B) LX dimensions, (C) LY dimensions, (D) LZ dimension.

The dark body factor F2 contributes over 80% to maximize green density. This result is consistent with literature review. Other works confirm that binder saturation strongly affects green density [10]. It is expected that increasing the amount of binder increases the mass of sample, since binder occupies a higher volume of voids between particles. Powder applicator speed is the second most influencing factor affecting green density; in fact, rake speed influences particles arrangement, particle migration, and packing density, as shown by DEM simulation [23].

As shown in Fig. 3(B), dimensions aligned with binder injection direction (X) are highly influenced by shell thickness F4, both external and internal dimensions. Fig. 2 also shows that LX-ext accuracy increases on increasing printhead speed. This was unexpected since ballistic effect of droplets is considered a source of lack of accuracy on X direction. Other origin of inaccuracy will be explored considering the influence of curing and de-powdering. Considering LX-int, strong effect of dark body F2 is also observed.

External features aligned with powder spreading (Y) are mainly influenced by printhead speed F1. On the other hand, internal features are equally affected by dark body F2, rake speed F3, and shell thickness F4, so that there is not a dominant factor. Same conclusion can be derived from Fig. 3(D) regarding the inaccuracy of LZ. There is a slightly higher contribution of printhead speed F1, which provides the lower error by using the higher speed level according to Fig. 2. The higher printing speed likely determines better absorption of binder in the layer thickness. For this reason, a minor number of extra particles are bonded, creating a smaller positive offset as reported in Table 4.

Table 5 reports the fitting coefficients calculated by the linear regression analysis defined by equation (5). The adjust coefficient of determination (R-sq Adj) was also calculated for checking the goodness of the linear regression. Virtually reliable results were found for density and LX-int, which showed significant contribution of dark body and shell thickness, respectively, as discussed in ANOVA analysis. Despite the poor R-sq Adj coefficient of other response variables, the model can be the basis for a multi-objective optimization.

Table 5. fitting coefficients resulting by the linear regression model expressed by equation (5).

Response variable	α	β	γ	δ	ζ	R-sq Adj
Density	4.587	0	5.43e-2	1.059e-2	1.12e-2	83.20%
LX ext	0.762	-7.35e-4	5.57e-3	-3.15e-3	-2.624e-2	51.92%
LX int	1.138	-1.18e-4	2.253e-2	6.42e-3	-2.721e-2	70.95%
LY ext	0.342	-7.33e-4	-8.8e-4	-3.69e-3	-2.2e-3	46.03%
LY int	0.640	1.43e-3	2.18e-2	-1.417e-2	-4.1e-3	24.20%
LZ	0.848	-1.935e-3	1.03e-2	-7.23e-3	3.9e-3	28.01%

4 Conclusions

This work investigates the optimization of binder jetting printing process. Taguchi method was adopted to study the influence of four factors (printhead speed, dark body, powder spreading speed and shell thickness) on three levels. Green density and dimensional inaccuracy were used as response variables. Here are the main findings:

- Green density varied between 0.53 and 0.57% of relative density. Dark body has the highest contribution, over 80%, as it controls the amount of binder deposited.
- Dimensional inaccuracy varied between 0.53% and -1.01%. Higher accuracy was found along external feature aligned with powder spreading direction (Y). Dimensions aligned with powder spreading (Z) present slightly higher accuracy than those aligned with binder injection (X) and powder spreading directions. Printhead speed has the highest contribution, and inaccuracy is minimized at higher printing speed.
- In the building plane, significantly better accuracy was found along powder spreading (Y) than binder injection (X). Moreover, external features are largely better than inner features. Based on ANOVA, shell thickness plays the major role in inaccuracy along X. Y dimensions are mainly affected by printhead speed. According to literature, the ballistic effect of droplets during the deposition can explain such differences but not exhaustively. Other sources might affect the lack of precision, such as curing and de-powdering.

Finally, a linear regression model was proposed to identify the best printing parameter combination through a multi-objective analysis. On the basis of the SNR and ANOVA analysis, the optimal levels can be proposed distinguishing between green density and geometrical accuracy. The optimal levels to maximize green density are: speed 150 mm/s, dark body setting 6, powder applicator speed 25 mm/s, and shell thickness 1 pixel. In contrast, the best dimensional accuracy can be achieved with speed 250 mm/s, dark body setting 0, powder applicator speed 38 mm/s, and shell thickness 5 pixels.

Future works will be directed towards experimentally verifying the optimal levels identified in this study, also aiming at investigating the possibility of highlighting good (even if not optimal) values for both green density and dimensional accuracy. Moreover, dedicated and experimental campaigns should be conducted to clarify the hypotheses explaining the influence of printing parameters on the dimensional accuracy.

Acknowledgements

The project is financed by Provincia Autonoma di Trento, L.P. 13/12/1999, n. 6, Art. 5: Aiuti per la promozione della ricerca e sviluppo. Authors are grateful to dr. Matteo Perina and the whole staff of Mimest s.p.a. for producing the samples and fruitfully cooperating.

References

1. ASTM-F2792-12A: Standard Terminology for Additive Manufacturing Technologies. ASTM Int. 5–7 (2012).
2. Ziaee, M., Crane, N.B.: Binder jetting: A review of process, materials, and methods. Addit. Manuf. 28, 781–801 (2019).
3. Chadha, U., Abrol, A., Vora, N.P., Tiwari, A., Shanker, S.K., Selvaraj, S.K.: Performance evaluation of 3D printing technologies: a review, recent advances, current challenges, and future directions. Springer International Publishing (2022).
4. Zago, M., Lecis, N., Mariani, M., Cristofolini, I.: Analysis of the causes determining dimensional and geometrical errors in 316L and 17 - 4PH stainless steel parts fabricated by metal binder jetting. Int. J. Adv. Manuf. Technol. (2024).
5. Zago, M., Cristofolini, I., Amirabdollahian, S.: Designing Powder Metallurgy Process - The Influence of High Sintering Temperature on Dimensional and Geometrical Precision. In: Lecture Notes in Mechanical Engineering. pp. 3–8 (2021).
6. Zago, M., Perina, M., Cristofolini, I.: Preliminary Design Method Accounting for Shape Distortion in Metal Binder Jetting Parts: A Case Study. In: Gerbino, S., Lanzotti, A., Martorelli, M., Mirálbes Buil, R., Rizzi, C., and Roucoules, L. (eds.) Lecture Notes in Mechanical Engineering. pp. 925–936. Springer International Publishing, Cham (2023).
7. Zago, M., Cristofolini, I.: Assessment of the Achievable Dimensional Tolerances in 17-4PH Stainless Steel Parts Fabricated by Metal Binder Jetting. Lect. Notes Mech. Eng. 31 – 40 (2024).

8. Barthel, B., Janas, F., Wieland, S.: Powder condition and spreading parameter impact on green and sintered density in metal binder jetting. Powder Metall. 0, 1–9 (2021).
9. Wang, Y., Zhao, Y.F.: Investigation of Sintering Shrinkage in Binder Jetting Additive Manufacturing Process. Procedia Manuf. 10, 779–790 (2017).
10. Chen, W., Chen, Z., Chen, L., Zhu, D., Fu, Z.: Optimization of Printing Parameters to Achieve High-Density 316L Stainless Steel Manufactured by Binder Jet 3D Printing. J. Mater. Eng. Perform. 32, 3602–3616 (2023).
11. Shrestha, S., Manogharan, G.: Optimization of Binder Jetting Using Taguchi Method. Jom. 69, 491–497 (2017).
12. Lores, A., Azurmendi, N., Agote, I., Espinosa, E., García-Blanco, M.B.: A study of parameter and post-processing effects on surface quality improvement of Binder Jet 3D-printed Invar36 alloy parts. Prog. Addit. Manuf. 7, 917–930 (2022).
13. Chen, H., Zhao, Y.F.: Process parameters optimization for improving surface quality and manufacturing accuracy of binder jetting additive manufacturing process. Rapid Prototyp. J. 22, 527–538 (2016).
14. Mendoza Jimenez, E., Ding, D., Su, L., Joshi, A.R., Singh, A., Reeja-Jayan, B., Beuth, J.: Parametric analysis to quantify process input influence on the printed densities of binder jetted alumina ceramics. Addit. Manuf. 30, (2019).
15. Hsu, T.J., Lai, W.H.: Manufacturing parts optimization in the three-dimensional printing process by the Taguchi method. J. Chinese Inst. Eng. Trans. Chinese Inst. Eng. A/Chung-kuo K. Ch'eng Hsuch K'an. 33, 121–130 (2010).
16. Zago, M., Lecis, N., Mariani, M., Cristofolini, I.: Analysis of the Flatness Form Error in Binder Jetting Process as Affected by the Inclination Angle. Metals (Basel). 12, (2022).
17. Zago, M., Lecis, N., Mariani, M., Uçak, O.U., Cristofolini, I.: Influence of shape distortion on the precision of holes in parts fabricated by Metal Binder Jetting. Int. J. Interact. Des. Manuf. (2023).
18. Dahmen, T., Henriksen, N.G., Dahl, K. V., Lapina, A., Pedersen, D.B., Hattel, J.H., Christiansen, T.L., Somers, M.A.J.: Densification, microstructure, and mechanical properties of heat-treated MAR-M247 fabricated by Binder Jetting. Addit. Manuf. 39, (2021).
19. Montgomery, D.C.: Design and analysis of experiments. John wiley \& sons (2017).
20. Ziaee, M., Crane, N.B.: Binder jetting: A review of process, materials, and methods. Addit. Manuf. 28, 781–801 (2019).
21. Li, M., Du, W., Elwany, A., Pei, Z., Ma, C.: Metal Binder Jetting Additive Manufacturing: A Literature Review. J. Manuf. Sci. Eng. 142, 1–17 (2020).
22. Parab, N.D., Barnes, J.E., Zhao, C., Cunningham, R.W., Fezzaa, K., Rollett, A.D., Sun, T.: Real time observation of binder jetting printing process using high-speed X-ray imaging. Sci. Rep. 9, 1–10 (2019).
23. Lee, Y., Gurnon, A.K., Bodner, D., Simunovic, S.: Effect of Particle Spreading Dynamics on Powder Bed Quality in Metal Additive Manufacturing. Integr. Mater. Manuf. Innov. 9, 410–422 (2020).